

State Variable Decoupling and Power Flow Control in PWM Current-Source Rectifiers

José R. Espinoza, *Member, IEEE*, and Géza Joós, *Senior Member, IEEE*

Abstract—Pulsewidth modulated (PWM) current-source rectifiers (CSR), among other alternatives, offer marked improvements over thyristor line-commutated rectifiers as a source of variable dc power. Advantages include reduced line current harmonic distortion and complete displacement power factor control, including unity displacement power factor operation. However, due to nonlinearities of the PWM-CSR model, their control has usually been carried out using direct line current control in a three-phase stationary frame (abc). This paper proposes the application of a nonlinear control technique that introduces more flexibility in the control of the rectifier and results in a more straightforward approach to controller design. The proposed technique is based on a nonlinear state variable feedback approach in the rotating frame (dq). The approach allows the independent control of the two components of the line current (active and reactive) with the same dynamic performance, regardless of the operating point. The control strategy also eliminates the need for input damping resistors and rejects the effect of supply voltage variations. Furthermore, a space vector modulation (SVM) technique is used to maximize the supply voltage utilization. This paper includes a complete formulation of the system equations and a controller design procedure. Experimental results on a 2-kVA digital-signal-processor-controlled prototype confirm the validity of theoretical considerations.

Index Terms—Current-source rectifier, decoupled control, dq rotating frame, input-output linearization, on-line control, pulsewidth modulated, space vector.

I. INTRODUCTION

THE use of line-commutated thyristor rectifiers as front-end ac/dc converters presents a number of drawbacks, including poor power factor and high-input current harmonic distortion. Pulsewidth modulated current-source rectifiers (PWM-CSR's), among other alternatives, offer a solution to these drawbacks. In such rectifiers, a smoothing reactor is placed on the dc side and an LC filter is inserted on the ac side to reduce the current harmonic injection resulting from the PWM operation. Direct interfacing with the ac mains often requires stringent specifications. They include high-input displacement power factor (DPF: cosine of the angle between the supply voltage and the fundamental line current component; ideally,

≈ 1) and low input current distortion factor (DF: rms current harmonic content to rms fundamental current component; ideally, ≈ 0). If the supply voltages are sinusoidal and both requirements are met, unity input power factor is achieved.

In conventional control schemes, the PWM-CSR has been operated with off-line patterns [1]–[2], which simplifies the compliance of the gating signals with the special requirements of switches in current-source (CS) converters (shorting pulses and overlaps). On the other hand, the presence of the LC input filter results in a load-dependent input DPF and may produce transient oscillations [3]. Although oscillations can be attenuated by adding damping resistors, these reduce the overall conversion efficiency.

To overcome the above drawbacks, several control strategies that operate the rectifier by means of on-line current control have been proposed in [4]–[8]. The main goals have been to keep unity DPF, to reduce the value of the damping resistors, and to regulate either the dc voltage or the dc current. References [4] and [5] propose solutions that meet the main requirements by using state variable feedback compensation in the stationary abc frame, where the gating signals are successfully generated by using carrier-based analog modulating techniques. However, both control schemes allow only unity DPF operation and do not provide a means of controlling independently the reactive power. On the other hand, the success of the line current control loop implementation assumes that the input filter components values (C_i and L_i in Fig. 1) are known and time invariant, conditions that do not hold in most practical implementations. Reference [6] compensates for the input DPF by using a linear approximation; however, the analysis and design assume a 100-kHz switching frequency, which limits it to low-power applications. Reference [7] shows that active damping can be readily implemented by means of state variable feedback. Finally, [8] presents a simple and low-cost approach (it uses standard analog and digital electronics) to achieve near unity DPF; however, the carrier-based sinusoidal pulsewidth modulation (SPWM) technique presents low voltage utilization, the control strategy still exhibits a load-dependent DPF, and the power factor cannot be adjusted to an arbitrary value.

Among other recent developments, space vector modulation (SVM) has been shown to have a high voltage gain, reduced switching frequency, low line current harmonic distortion, and a straightforward implementation on digital systems [9]–[11]. Unlike linear controllers in the abc frame, it has also been demonstrated that the dq transformation provides an effective means of obtaining zero steady-state error [12].

Manuscript received July 15, 1996; revised April 29, 1997. The work of J. R. Espinoza was supported by the School of Graduate Studies of Concordia University under a Concordia University International Fee Remission Award and a Concordia University Graduate Fellowship.

J. R. Espinoza was with the Department of Electrical and Computer Engineering, Concordia University, Montreal, P.Q., H3G 1M8 Canada. He is now with the Departamento de Ingeniería Eléctrica, Universidad de Concepción, Concepción, Chile (e-mail: jespinoz@manet.die.udec.cl).

G. Joós is with the Department of Electrical and Computer Engineering, Concordia University, Montreal, P.Q., H3G 1M8 Canada (e-mail: geza@ece.concordia.ca).

Publisher Item Identifier S 0278-0046(98)00497-3.

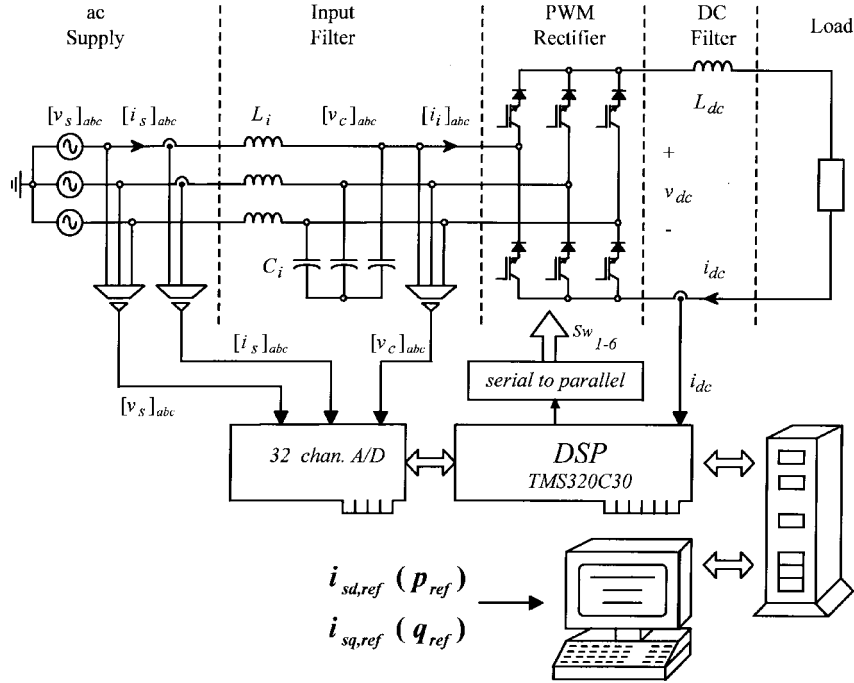


Fig. 1. PWM-CSR.

This paper proposes a control method based on a non-linear state variable feedback approach that introduces more flexibility in the control of the PWM-CSR and a more straightforward approach to controller design [13], [14]. The nonlinear technique has already been applied and has demonstrated its superiority in PWM voltage-source rectifiers [14]. Specifically, it consists of linearizing the dq state variable model of the system, decoupling, and controlling independently the direct (active power) and the quadrature (reactive power) line current components. Also, the SVM technique is used to generate the switching pattern. The following improved features are obtained: 1) independent control of the active and reactive power components; 2) inherent input filter damping (provided by the state variable feedback compensation loop); 3) fast transient response (limited only by the digital system sampling time); and 4) high supply voltage utilization and reduced switching frequency.

This paper includes the complete analysis and the design procedure of the proposed control strategy based on a non-linear state variable feedback approach. Experimental results on a 2-kVA digital-signal-processor (DSP)-based laboratory prototype are also included to confirm the feasibility of the proposed control scheme.

II. POWER TOPOLOGY

The complete power circuit, shown in Fig. 1, is composed of a three-phase PWM-CSR, a dc-link reactor (L_{dc}), and a three-phase second-order input filter (L_i, C_i). The main function of the PWM-CSR is to regulate the level of the dc-link current (i_{dc}) by adjusting the PWM-CSR dc-link bus voltage (v_{dc}). The harmonics injected into the ac mains by the PWM-CSR operation are minimized by the LC input filter. The dc-link reactor (L_{dc}) smoothes the dc-link current (i_{dc}) and, therefore,

acts as a current source to the PWM-CSR. Fig. 1 also shows the DSP-based setup used to implement the control strategy.

The magnitude of L_{dc} , C_i , and L_i depend upon the permissible dc-link current ripple, input capacitor voltage ripple, and the resonant frequency, respectively. They also depend upon the sample frequency of the PWM-CSR. Section VI presents complete design guidelines for these passive components.

III. PWM-CSR MODELING

A. Equivalent Model in the Stationary abc Frame

An equivalent single-phase circuit for the ac supply, input filter, and PWM-CSR and the dc equivalent circuit are shown in Fig. 2. The dc voltage (v_{dc}) and ac PWM-CSR line currents ($[i_i]_{abc} = [i_{ia} \ i_{ib} \ i_{ic}]^T$) are given by

$$v_{dc} = G_{ac}[m]_{abc}^T[v_c]_{abc} \quad (1)$$

$$[i_i]_{abc} = G_{ac}[m]_{abc}i_{dc} \quad (2)$$

where G_{ac} is the ac gain of the PWM technique ($G_{ac} = 1$ for the SVM) and $[m]_{abc} = [m_a \ m_b \ m_c]^T$ is the modulating vector (input variables).

Each phase of the circuit is modeled by using the state variable approach and, thereby, by using (1) and (2), the model of the system (Fig. 2) in the abc frame becomes

$$\frac{d}{dt}[i_s]_{abc} = -\frac{1}{L_i}[v_c]_{abc} + \frac{1}{L_i}[v_s]_{abc} \quad (3)$$

$$\frac{d}{dt}[v_c]_{abc} = \frac{1}{C_i}[i_s]_{abc} - \frac{1}{C_i}G_{ac}[m]_{abc}i_{dc} \quad (4)$$

$$\frac{d}{dt}i_{dc} = \frac{1}{L_{dc}}G_{ac}[m]_{abc}^T[v_c]_{abc} - \frac{R_{dc}}{L_{dc}}i_{dc} \quad (5)$$

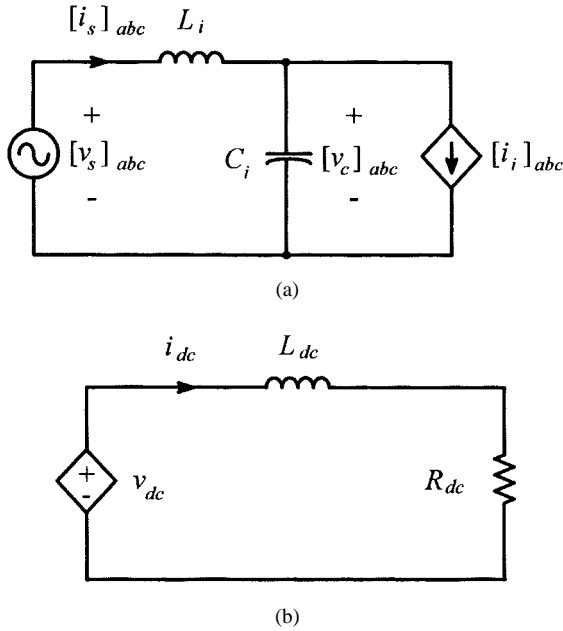


Fig. 2. PWM-CSR model in the abc frame. (a) AC side. (b) DC side.

where $[i_s]_{abc} = [i_{sa} \ i_{sb} \ i_{sc}]^T$, $[v_c]_{abc} = [v_{ca} \ v_{cb} \ v_{cc}]^T$, and i_{dc} are the state variables. The supply voltage vector $[v_s]_{abc} = [v_{sa} \ v_{sb} \ v_{sc}]^T$ is the perturbation variable.

The dq transformation is valid under steady-state and dynamic conditions [6]. In the dq frame and under steady-state conditions, all state variables become dc quantities. Standard integral (I) and proportional integral (PI) controllers can, therefore, be used to reduce the steady-state error to zero. The dc-loop feature also simplifies the design of the controllers used to meet transient requirements (i.e., overshoot and settling time). In addition, the control in the dq frame reduces the number of controllers from three (in the abc frame) to two. Finally, the d and q components are directly associated with real and reactive power components, thus simplifying the power flow control.

B. Equivalent Model in the Rotating dq Frame

In order to simplify the analysis, a balanced ac voltage supply is assumed, hence, the state variables only have d and q components, the zero-sequence component being equal to zero. Thus, the dq transformation of the model in abc coordinates (3)–(5) yields

$$\frac{d}{dt}[i_s]_{dq} + W[i_s]_{dq} = -\frac{1}{L_i}[v_c]_{dq} + \frac{1}{L_i}[v_s]_{dq} \quad (6)$$

$$\frac{d}{dt}[v_c]_{dq} + W[v_c]_{dq} = \frac{1}{C_i}[i_s]_{dq} - \frac{1}{C_i}G_{ac}[m]_{dq}i_{dc} \quad (7)$$

$$\frac{d}{dt}i_{dc} = \frac{3}{2} \frac{1}{L_{dc}}G_{ac}[m]_{dq}^T[v_c]_{dq} - \frac{R_{dc}}{L_{dc}}i_{dc} \quad (8)$$

where $[v_s]_{dq} = [v_{sd} \ v_{sq}]^T$ (supply dq voltage vector), $[i_s]_{dq} = [i_{sd} \ i_{sq}]^T$ (supply dq line current vector), $[v_c]_{dq} = [v_{cd} \ v_{cq}]^T$ (capacitor dq voltage vector), $[m]_{dq} = [m_d \ m_q]^T$ (input dq vector), ω is the supply angular frequency ($\omega = 2\pi 60 \approx 377$),

and

$$W = \begin{bmatrix} 0 & -\omega \\ \omega & 0 \end{bmatrix}.$$

By expanding the dq model (6)–(8) into its components yields

$$\frac{d}{dt}i_{sd} = \omega i_{sq} - \frac{1}{L_i}v_{cd} + \frac{1}{L_i}v_{sd} \quad (9)$$

$$\frac{d}{dt}i_{sq} = -\omega i_{sd} - \frac{1}{L_i}v_{cq} + \frac{1}{L_i}v_{sq} \quad (10)$$

$$\frac{d}{dt}v_{cd} = \omega v_{cq} + \frac{1}{C_i}i_{sd} - \frac{1}{C_i}G_{ac}i_{dc}m_d \quad (11)$$

$$\frac{d}{dt}v_{cq} = -\omega v_{cd} + \frac{1}{C_i}i_{sq} - \frac{1}{C_i}G_{ac}i_{dc}m_q \quad (12)$$

$$\frac{d}{dt}i_{dc} = \frac{3}{2} \frac{1}{L_{dc}}G_{ac}(m_d v_{cd} + m_q v_{cq}) - \frac{R_{dc}}{L_{dc}}i_{dc}. \quad (13)$$

The resulting model (9)–(13) represents a multiple-input multiple-output (MIMO) type of system. The inputs are the modulating variables (m_d, m_q), and the outputs are the quadrature (i_{sq} , reactive power) and the direct (i_{sd} , active power) components of the supply current. Note that unity DPF is a special case (when $i_{sq} = 0$, if a dq rotating frame synchronized with the supply voltages is assumed) and that the dc side of the rectifier can be considered as a current source with a value equal to i_{dc} .

Furthermore, the dq model of the PWM-CSR, (9)–(13), shows that the system is nonlinear [(11)–(13) contain multiplication of the input variables and the state variables] and coupled (for instance, (13) shows that the dc current depends upon both input variables). Thus, to decouple and linearize the model, an input–output linearization method is proposed [13]–[15]. This method provides a nonlinear transformation that is straightforward to derive. It is, therefore, preferred over input-state linearization, an alternative method of linearization which is more involved and requires a larger amount of mathematical derivations. Moreover, this strategy, unlike a small signal model approach, allows the decoupled control of the state variables with the same dynamic performance, regardless of the operating point (dc current level).

IV. PROPOSED CONTROL STRATEGY DESCRIPTION

A. Input–Output Linearization and Decoupling

The method in [15] differentiates the output variables as many times as necessary, until one or more input variables appear explicitly. Then, the input variables are designed to linearize and decouple the system dynamics. If i_{sd} is differentiated once, (9) is obtained, which does not contain any input. Therefore, it is differentiated again and, by using (10) and (11), yields

$$\begin{aligned} \frac{d^2}{dt^2}i_{sd} = & -i_{sd}(\omega^2 + \omega_r^2) - \frac{2\omega}{L_i}v_{cq} + \frac{\omega}{L_i}v_{sq} \\ & + \omega_r^2 G_{ac}i_{dc}m_d + \frac{1}{L_i} \frac{d}{dt}v_{sd} \end{aligned} \quad (14)$$

where $\omega_r = 1/\sqrt{C_i L_i}$ is the resonant angular frequency of the input filter.

Since (14) contains the input m_d , the differentiation process applied to i_{sd} stops here. The same procedure is applied to i_{sq} , which yields

$$\begin{aligned} \frac{d^2}{dt^2} i_{sq} = & -i_{sq}(\omega^2 + \omega_r^2) + \frac{2\omega}{L_i} v_{cd} - \frac{\omega}{L_i} v_{sd} \\ & + \omega_r^2 G_{ac} i_{dc} m_q + \frac{1}{L_i} \frac{d}{dt} v_{sq}. \end{aligned} \quad (15)$$

Equations (14) and (15) can be written in a matrix format as

$$\mathbf{X}(t) = \mathbf{A}(t) \cdot [\mathbf{m}]_{dq} + \mathbf{B}(t) \quad (16)$$

where $\mathbf{X}(t) = [(d^2/dt^2)i_{sd} \ (d^2/dt^2)i_{sq}]^t$, $\mathbf{A}(t) = G_{ac}\omega_r^2 i_{dc}$, and

$$\mathbf{B}(t) = \begin{bmatrix} -i_{sd}(\omega^2 + \omega_r^2) - \frac{2\omega}{L_i} v_{cq} + \frac{\omega}{L_i} v_{sq} + \frac{1}{L_i} \frac{d}{dt} v_{sd} \\ -i_{sq}(\omega^2 + \omega_r^2) + \frac{2\omega}{L_i} v_{cd} - \frac{\omega}{L_i} v_{sd} + \frac{1}{L_i} \frac{d}{dt} v_{sq} \end{bmatrix}.$$

The second step of the input–output linearization method is to force $\mathbf{X}(t)$ to be of the linear and decoupled form:

$$\mathbf{X}(t) = \mathbf{D} \cdot [\mathbf{u}]_{dq} + \mathbf{F}(t) \quad (17)$$

where \mathbf{D} and $\mathbf{F}(t)$ are conveniently defined as

$$\begin{aligned} \mathbf{D} &= k_2, \\ \mathbf{F}(t) &= \begin{bmatrix} -k_1 \frac{d}{dt} i_{sd} - k_2 i_{sd} \\ -k_1 \frac{d}{dt} i_{sq} - k_2 i_{sq} \end{bmatrix} \\ &= \begin{bmatrix} -k_1 \omega i_{sq} + \frac{k_1}{L_i} v_{cd} - \frac{k_1}{L_i} v_{sd} - k_2 i_{sd} \\ k_1 \omega i_{sd} + \frac{k_1}{L_i} v_{cq} - \frac{k_1}{L_i} v_{sq} - k_2 i_{sq} \end{bmatrix}. \end{aligned}$$

Also, $[u]_{dq}$ is a new dq set of input variables, and k_1 and k_2 are arbitrary positive gains used for pole placement.

The existence of the linear and decoupled form (17) is conditioned to the existence of the *input transformation* ($[\mathbf{m}]_{dq}$ as a function of $[u]_{dq}$). The expression of the *input transformation* is obtained by equalizing (16) and (17). Hence,

$$\begin{aligned} [\mathbf{m}]_{dq} &= \mathbf{A}^{-1}(t) \cdot (\mathbf{D}[u]_{dq} + \mathbf{F}(t) - \mathbf{B}(t)) \\ &= \underbrace{\frac{1}{G_{ac}\omega_r^2 i_{dc}}}_{\text{linearization}} \left\{ k_2 \begin{bmatrix} u_d \\ u_q \end{bmatrix} + \underbrace{\begin{bmatrix} -k_1 \frac{d}{dt} i_{sd} - k_2 i_{sd} \\ -k_1 \frac{d}{dt} i_{sq} - k_2 i_{sq} \end{bmatrix}}_{\text{damping}} \right. \\ &\quad \left. - \underbrace{\begin{bmatrix} -i_{sd}(\omega^2 + \omega_r^2) - \frac{2\omega}{L_i} v_{cq} + \frac{\omega}{L_i} v_{sq} + \frac{1}{L_i} \frac{d}{dt} v_{sd} \\ -i_{sq}(\omega^2 + \omega_r^2) - \frac{2\omega}{L_i} v_{cd} + \frac{\omega}{L_i} v_{sd} + \frac{1}{L_i} \frac{d}{dt} v_{sq} \end{bmatrix}}_{\text{decoupling}} \right\} \\ &\quad \underbrace{\begin{bmatrix} -i_{sd}(\omega^2 + \omega_r^2) - \frac{2\omega}{L_i} v_{cq} + \frac{\omega}{L_i} v_{sq} + \frac{1}{L_i} \frac{d}{dt} v_{sd} \\ -i_{sq}(\omega^2 + \omega_r^2) - \frac{2\omega}{L_i} v_{cd} + \frac{\omega}{L_i} v_{sd} + \frac{1}{L_i} \frac{d}{dt} v_{sq} \end{bmatrix}}_{\text{voltage rejection}} \end{aligned} \quad (18)$$

The expression for the modulating vector (18) shows one possible singularity ($i_{dc} = 0$). Under this condition, the *input transformation* is not defined and, thereby, the method cannot be applied. However, although $i_{dc} = 0$ could be achieved during transient conditions, it is not a normal operation mode. Equation (18) also shows the different terms that contribute to

the linearization, damping, decoupling, and rejection of supply voltage variations.

On the other hand, the actual implementation of (18) requires the differential of the d and q component of the supply voltages. In practice, since the supply voltage signals have superimposed noise, they are filtered by means of analog filters (cutoff frequency of about 10 kHz), then sampled, and finally numerically differentiated. Note that $\mathbf{F}(t)$ in (18) can be implemented using the sampled state variables (17) and, thus, the differential of the supply line currents are not required.

The last step of the method is to analyze the stability of the *internal dynamics*. Since the method requires differentiating i_{sd} and i_{sq} twice, the *total relative degree* of the system is four [15]. Therefore, there is just one *internal dynamics* (the one associated with i_{dc}) to be tested for stability (since the dimension of the system is five). The Appendix shows that i_{dc} is always bounded in the PWM-CSR operating region (Section V). Thus, the control law yields a stable closed-loop system.

Thus, the direct and quadrature line currents can be independently controlled by means of u_d and u_q , respectively, and with the same dynamic performance in the PWM-CSR operating region.

B. Dynamic Response Optimization

Since the resulting system model in (17) is linear, the Laplace transform is used to continue the analysis and design. Thus, the model in (17) can be expanded and written as follows:

$$\frac{I_{sd}(s)}{U_d(s)} = \frac{I_{sq}(s)}{U_q(s)} = \frac{k_2}{s^2 + sk_1 + k_2} \quad (19)$$

where $I_{sd}(s)$, $I_{sq}(s)$, $U_d(s)$, and $U_q(s)$ are the Laplace transforms of i_{sd} , i_{sq} , u_d , and u_q , respectively.

The Laplace transform of the model in (19) shows that zero steady-state error in both current loops should be expected. This is valid as long as the *input transformation* (18) is computed accurately, which assumes knowing the exact value of ω_r or L_i and C_i . These values are usually available as approximations, therefore, zero steady-state error is not totally assured. In order to achieve this, it is proposed to add two external integrators to force the steady-state error to zero, even for inaccurate values of C_i and L_i .

By adding a feedback loop with an integrator ($1/sT_{ac}$), the direct and quadrature line current closed-loop transfer functions become (Fig. 3):

$$\frac{I_{sd}(s)}{I_{sd,ref}(s)} = \frac{I_{sq}(s)}{I_{sq,ref}(s)} = \frac{k_2/T_{ac}}{s^3 + s^2k_1 + sk_2 + k_2/T_{ac}}. \quad (20)$$

The optimum third-order transfer function based on the itae criterion [16] is

$$\frac{(7.54/t_s)^3}{s^3 + 1.75(7.54/t_s)s^2 + 2.15(7.54/t_s)^2s + (7.54/t_s)^3} \quad (21)$$

where t_s is the design settling time for a 2% band.

Thus, if $t_{s,ac}$ is the desired settling time and the actual total model of the system (20) is equalized to the optimum third-order transfer function (21), the expressions for k_1 , k_2 , and

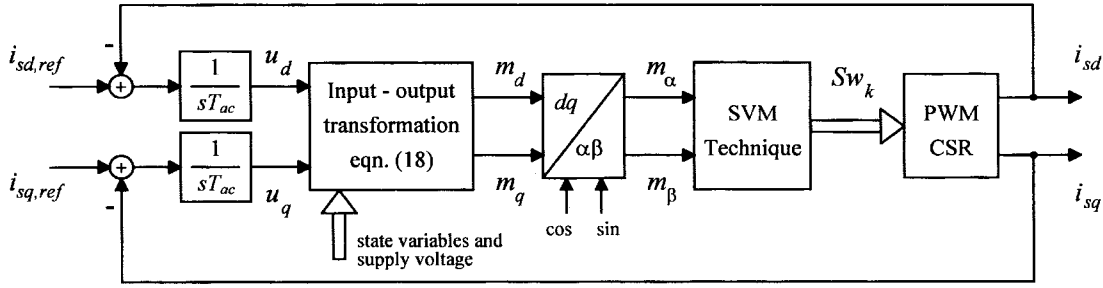


Fig. 3. Proposed control strategy (linearization, decoupling, and dynamic optimization).

T_{ac} are

$$k_1 = 1.75 \frac{7.54}{t_{s,ac}}, \quad k_2 = 2.15 \left(\frac{7.54}{t_{s,ac}} \right)^2, \quad T_{ac} = 2.15 \frac{t_{s,ac}}{7.54}. \quad (22)$$

V. PWM-CSR OPERATING REGION

The power topology and control strategy restrict the maximum and minimum steady-state values of the state variables and, thereby, the limits for the set-point references. For instance, due to the nature of the power circuit topology, the dc current is always positive; also, it will be shown that the quadrature line current range depends upon the actual dc current. Thus, to avoid setting the converter on an unachievable operating point, the operating region of the PWM-CSR is derived.

In order to find the steady-state operating region, the left-hand side of the model in dq coordinates (9)–(13) are set equal to zero and then solved systematically. The resulting set of variables are dc quantities and are designated by capital letters. Assuming the dq transformation is synchronized with the supply voltage ($V_{sq} = 0$), the resulting normalized expressions as a function of the inputs (M_d, M_q) are as follows:

$$I_{dc} = G_{ac} M_d \frac{f_{rn}^2}{f_{rn}^2 - 1} \text{ p.u.} \quad (23)$$

$$I_{sq} = \frac{(G_{ac} M_d M_q X_{Ci} f_{rn}^2 + f_{rn}^2 - 1) f_{rn}^2}{X_{Ci} (f_{rn} - 1)^2 (f_{rn} + 1)^2} \text{ p.u.} \quad (24)$$

$$I_{sd} = G_{ac}^2 \frac{f_{rn}^4}{(f_{rn} - 1)^2 (f_{rn} + 1)^2} (M_d)^2 \text{ p.u.} \quad (25)$$

$$V_{cq} = -G_{ac}^2 X_{Ci} \frac{f_{rn}^2}{(f_{rn} - 1)^2 (f_{rn} + 1)^2} (M_d)^2 \text{ p.u.} \quad (26)$$

$$V_{cd} = \frac{(G_{ac} M_d M_q X_{Ci} + f_{rn}^2 - 1) f_{rn}^2}{X_{Ci} (f_{rn} - 1)^2 (f_{rn} + 1)^2} \text{ p.u.} \quad (27)$$

where $f_{rn} = \omega_r/\omega$, $V_{base} = V_{sd}$, $I_{base} = 3V_{sd}/(2R_{dc})$, and X_{Ci} is the per unit (p.u.) capacitor reactance.

The inputs M_d and M_q are bounded. This comes from the fact that, in order to inject line currents ($[i]_{abc}$, Fig. 1) without distortion, the modulating vector (m_α, m_β , Fig. 3) must have a magnitude lower than or equal to one. This restriction in the dq frame can be expressed as

$$(M_q)^2 + (M_d)^2 \leq 1. \quad (28)$$

On the other hand, since the power topology (Fig. 1) can only provide positive dc currents, by using (23) and (28), one

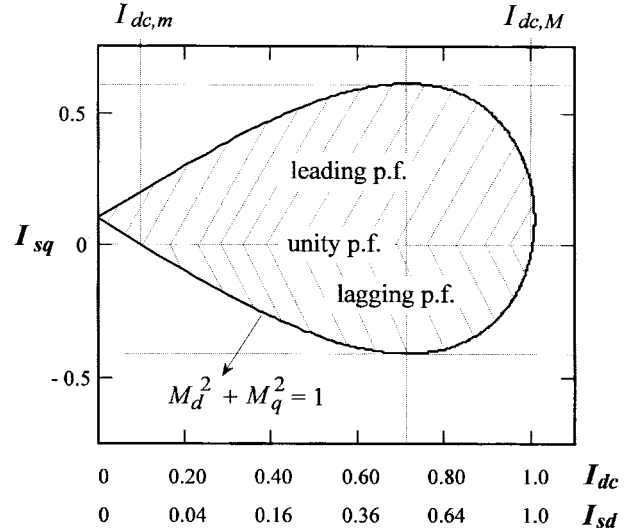


Fig. 4. Normalized operating region of the PWM-CSR (dc-link current (I_{dc}) versus quadrature line current (I_{sq}) for $C_i = 50$ mF, $L_i = 3$ mH, $R_{dc} = 20$ W, and $G_{ac} = 1$).

can finally write

$$0 \leq M_d \leq 1, \quad -1 \leq M_q \leq 1. \quad (29)$$

The ranges expressed in (29) define the boundary of the operating region and, thereby, the maximum and minimum set points for both direct and quadrature line current references. A graphical interpretation for the operating region is given in Fig. 4. From Fig. 4 and (23)–(29), it can be concluded that: 1) the range of the quadrature line current is restricted by the actual value of the dc current (Fig. 4), noting that the maximum range is given when $M_d = 0.707$; 2) the maximum dc current (23) is proportional to the ac gain of the modulating technique (G_{ac}) and independent of the resonant frequency of the input filter (f_{rn}) for $f_{rn} \gg 1$; and 3) unity DPF ($I_{sq} = 0$ in Fig. 4) can be achieved within a limited range of the dc-link current ($I_{dc,m} < I_{dc} < I_{dc,M}$, Fig. 4). In order to find the dc-link current range, which allows unity DPF, $f_{rn} \gg 1$ is assumed and (24) is equated to zero. Thus, from (23), the maximum dc-link current for unity DPF is $I_{dc,M} = 1$ and the minimum, $I_{dc,m}$, is given by

$$I_{dc,m} = G_{ac} \sqrt{\frac{1 - \sqrt{1 - 4/(G_{ac} X_{Ci})^2}}{2}} \text{ p.u.} \quad (30)$$

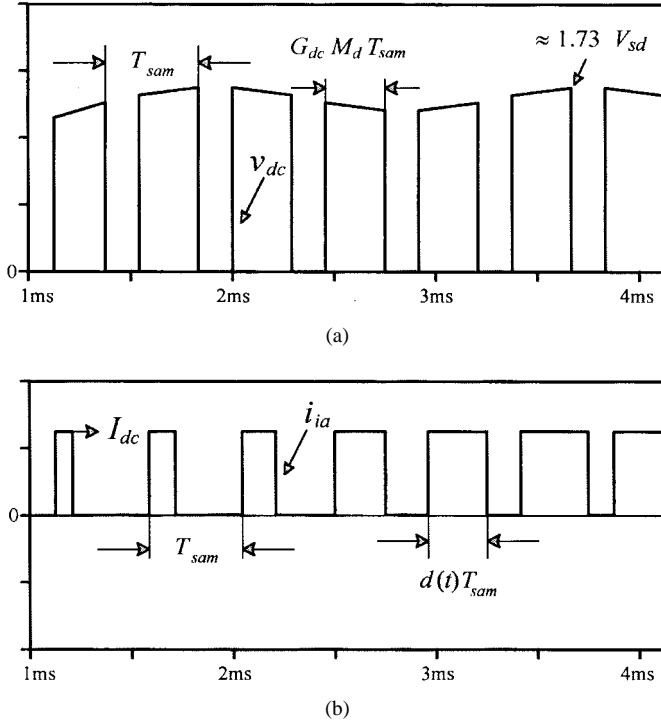


Fig. 5. Approximated CSR waveforms for filtering component design purposes. (a) DC-bus voltage (vdc). (b) AC line current (phase a, i_{ia}).

VI. DESIGN GUIDELINES FOR FILTERING COMPONENTS

In order to simplify the design of L_{dc} and C_i , a maximum peak-to-peak ripple criterion is used. On the other hand, L_i is designed to obtain a desired resonant frequency of the input ac filter. Thus, it is possible to avoid any resonance due to the PWM operation of the CSR (harmonics around $N, 2N, \dots$, where N is the normalized sample frequency), and noncharacteristic harmonics (fifth, seventh, \dots) due to instantaneous saturation of the controllers, which yields overmodulation.

The approximated PWM-CSR dc-bus voltage (v_{dc}) is depicted in Fig. 5(a). The design of the dc-link inductor is done to assure a small peak-to-peak dc-link current (i.e., 20% of the nominal dc-link current). Hence, if the voltage harmonics injected from the load side are neglected (as in the case of resistive or dc-drive loads), the peak-to-peak dc current (Δi_{dc}) can be expressed by

$$\Delta i_{dc} = \frac{\sqrt{3}V_{sd}}{L_{dc}} G_{dc} M_d T_{sam} = k_{Ldc} I_{dc} \quad (31)$$

where G_{dc} is the dc gain of the modulating technique ($G_{dc} = 0.866$, for the SVM), T_{sam} is the sample period of the SV ($= 1/(f_s N)$), f_s is the supply frequency ($f_s = 60$ Hz), and k_{Ldc} is a constant to fix the permissible dc current ripple ($k_{Ldc} = 0.20$ p.u.).

By using (23) and (31) and assuming $f_{rn}^2 \gg 1$, the normalized dc inductor reactance is given by

$$X_{Ldc} = \frac{2\pi\sqrt{3}}{k_{Ldc}N} \frac{G_{dc}}{G_{ac}} \text{ pu.} \quad (32)$$

The ac capacitor (C_i) is designed to meet a given peak-to-peak voltage ripple requirement across the input capacitor

($\Delta v_{C_i} = k_{C_i} V_{sd}$). The worst case design is when all current harmonics ($[i]_{abc}$) are absorbed by the ac capacitor [Fig. 5(b)]. This condition assumes that the frequencies of the harmonics injected by the PWM operation of the CSR are higher than the resonant frequency of the input filter ($N > f_{rn}$). Thus, the voltage ripple is given by

$$\Delta v_{C_i} = \frac{I_{dc}}{C_i} d(t) T_{sam} = k_{C_i} V_{sd}. \quad (33)$$

Although $d(t)$ is a function of time [Fig. 5(b)], the worst case ripple corresponds to $d(t) = 0.5$. Thus, by using (23) and (33), assuming $f_{rn}^2 \gg 1$ and maximum dc current (worst case), the normalized ac capacitor reactance is given by

$$X_{C_i} = \frac{k_{C_i} N}{\pi} \text{ p.u.} \quad (34)$$

Finally, the ac inductor (L_i) is calculated using a desired normalized resonant frequency for the input filter (f_{rn}). The resonant frequency (f_{rn}) is usually chosen lower than half of the normalized sample frequency (N) and higher than low frequencies due to transient overmodulation (fifth, seventh). Thus, the reactance is given by

$$X_{L_i} = X_{C_i} / f_{rn}^2 \text{ p.u.} \quad (35)$$

VII. EXPERIMENTAL RESULTS

A. Power Topology and Control Scheme Description

The power topology and proposed control strategy have been implemented on a 2-kVA laboratory prototype unit to verify feasibility (Fig. 1). A digital system based on the TMS320C30 DSP microprocessor has been used to implement the control strategy. The digital system uses a 32-channel A/D board to sample the required state variables. The main board executes the control algorithm and also performs other tasks, such as an on-line communication with a user interface, which runs on a PC platform. Thus, the references and controller parameters can be externally on-line entered and/or modified to perform transient and/or static tests. The gating signals are sent to the drivers through the serial port of the DSP microprocessor.

The gating signals are digitally generated using the SVM technique. This technique is preferred, due to its high supply voltage utilization (ac gain equal to 1), reduced switching frequency (equal to one half of the sample frequency), and straightforward implementation in digital systems [11]. The technique selects three switching combinations of the converter and their respective on times every sample time. The selection and on-time calculations are based upon the input modulation variables m_α and m_β (Fig. 3). The switching combinations are then sequentially applied to the PWM-CSR [9]. The technique can also readily include the shorting pulses that are needed when zero line currents at the ac side ($[i]_{abc}$) of the PWM-CSR are required.

Leading DPF is obtained by setting $i_{sq,ref} = 3$ A and $i_{sd,ref} = 4$ A (Fig. 7). The input line current (i_{sa}) is leading the supply phase voltage by approximately 36° [Fig. 7(a)]. The overall input power factor was 0.795 leading.

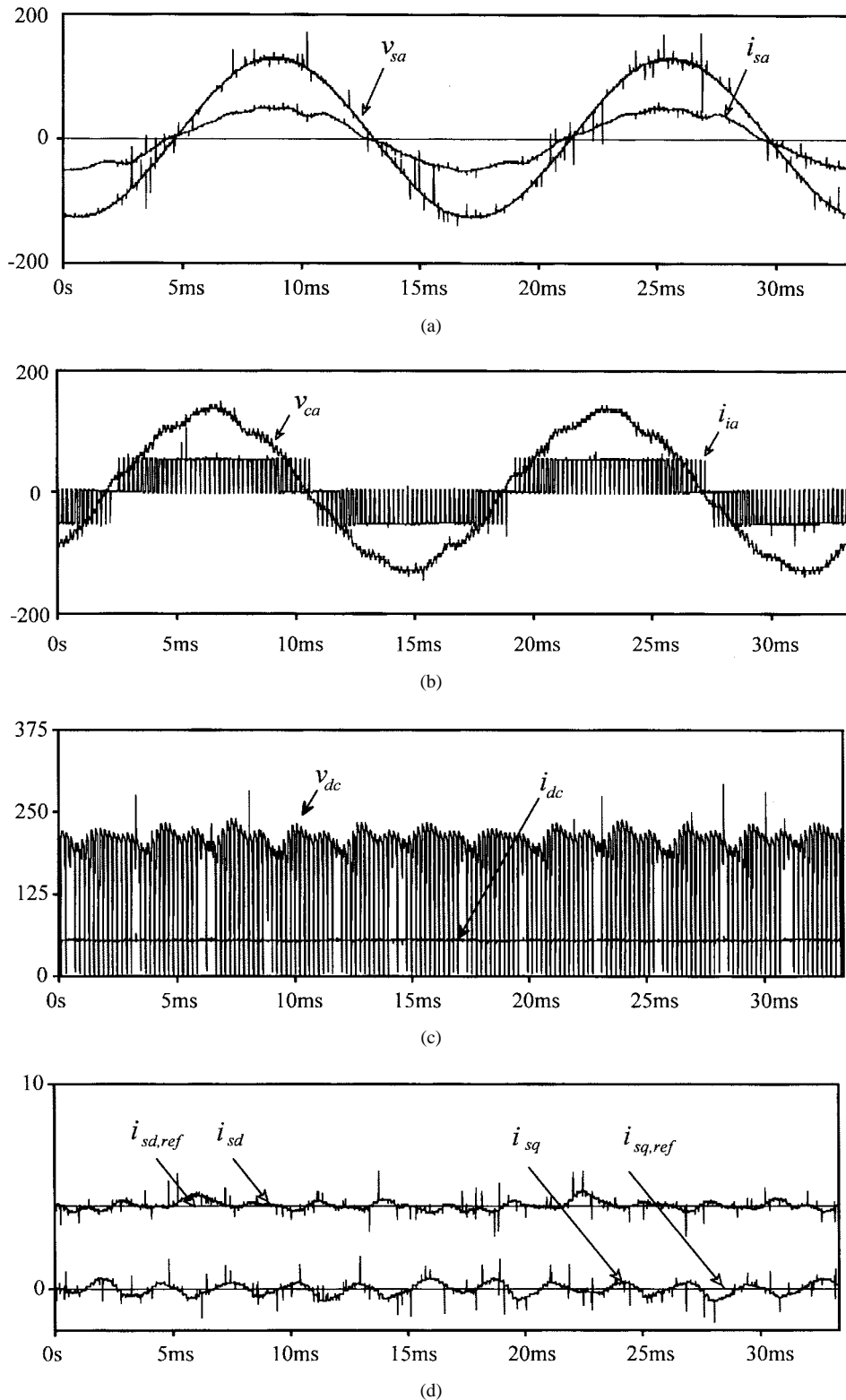


Fig. 6. PWM-CSR unity DPF operating mode ($i_{sd,ref} = 4$ A, $i_{sq,ref} = 0$), experimental waveforms (see Fig. 1). (a) Supply voltage (v_{sa}) and supply current ($10 i_{sa}$). (b) Capacitor voltage (v_{ca}) and ac CSR current ($10 i_{ia}$). (c) CSR dc-bus voltage (v_{dc}) and dc-link bus current ($10 i_{dc}$). (d) q and d line current references ($i_{sq,ref}$, $i_{sd,ref}$) and q and d actual line currents (i_{sq} , i_{sd}).

B. Filter Components and Controller Parameters Design

The minimum sample time in this setup is $185 \mu\text{s}$. Therefore, a sample frequency of 5040 Hz (sample period of $198 \mu\text{s}$) is chosen ($N = 84$). Both d and q line current controllers are designed to achieve a 5-ms settling time ($t_{s,ac} = 5$ ms).

Thus, by using (22), $k_1 = 2.639$ k, $k_2 = 4.892$ M, and $T_{ac} = 1.425$ m.

The selection of L_{dc} , C_i , and L_i is done by following the design guidelines provided in Section VI. Thus, assuming $k_{Ldc} = 0.20 (\cong 20\%$ peak-to-peak current ripple under the worst

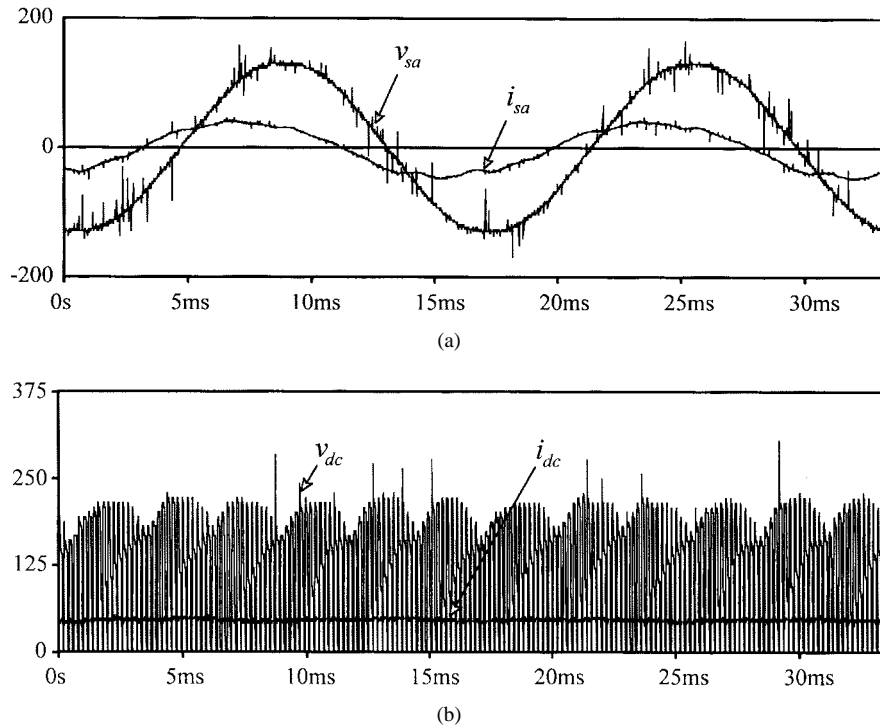


Fig. 7. PWM-CSR leading DPF operating mode ($i_{sd,ref} = 4$ A, $i_{sq,ref} = 3$ A, power factor = 0.8), experimental waveforms (see Fig. 1). (a) Supply phase voltage (v_{sa}) and supply current ($10 i_{sa}$). (b) CSR dc-bus voltage (v_{dc}) and dc-link bus current ($10 i_{dc}$).

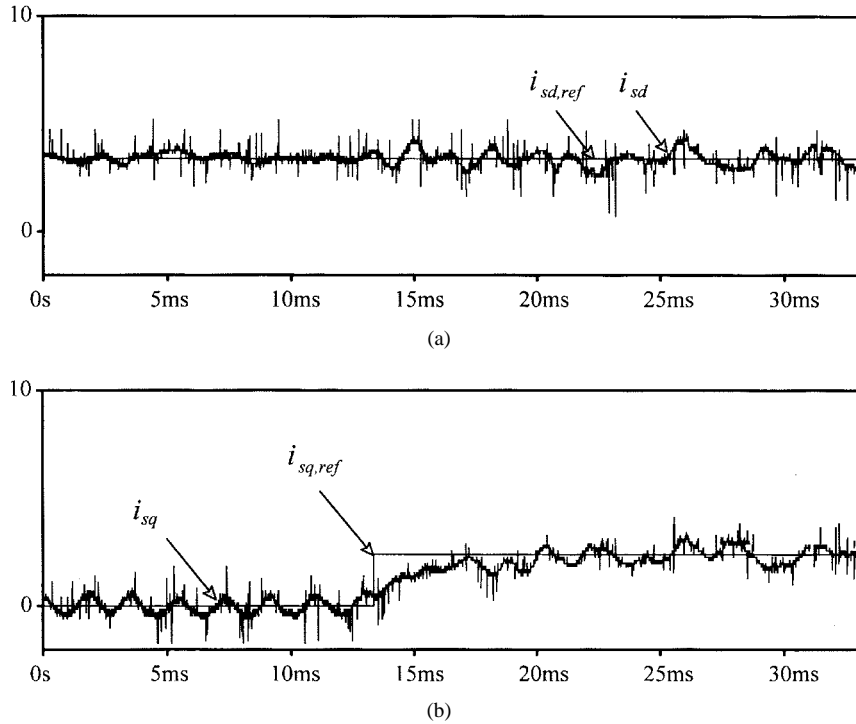


Fig. 8. PWM-CSR transient operating mode (from unity to leading DPF), experimental waveforms (see Fig. 1). (a) d reference ($i_{sd,ref}$) and d actual line current (i_{sd}). (b) q reference ($i_{sq,ref}$) and q actual line current (i_{sq}).

conditions), (32) yields $X_{Ldc} = 0.583 \Omega$ pu ($L_{dc} = 18.04$ mH). If $k_{Ci} = 0.20$ ($\cong 20\%$ peak-to-peak voltage ripple under the worst conditions), (34) yields $X_{Ci} = 5.347$ p.u. ($C_i = 42.52 \mu\text{F}$). Finally, the resonant frequency is chosen equal to nine ($f_{rn} = 9$), thus, (35) yields $X_{Li} = 0.066 \Omega$ p.u. ($L_i = 2.04$ mH). Due to practical limitations, the actual values used

in the experimental tests are $L_{dc} = 18$ mH, $C_i = 50 \mu\text{F}$, and $L_i = 3$ mH.

C. Experimental Waveforms

Unity DPF is achieved by setting $i_{sq,ref} = 0$ ($i_{sd,ref} = 4$ A, Fig. 6) since the dq rotating frame is synchronized with the ac

$$[m]_{dq} = \frac{1}{G_{ac}\omega_r^2 i_{dc}} \begin{bmatrix} \frac{d^2}{dt^2} i_{sd} + i_{sd}(\omega^2 + \omega_r^2) + \frac{2\omega}{L_i} v_{cq} - \frac{\omega}{L_i} v_{sq} - \frac{1}{L_i} \frac{d}{dt} v_{sd} \\ \frac{d^2}{dt^2} i_{sq} + i_{sq}(\omega^2 + \omega_r^2) - \frac{2\omega}{L_i} v_{cd} + \frac{\omega}{L_i} v_{sd} - \frac{1}{L_i} \frac{d}{dt} v_{sq} \end{bmatrix} \quad (A2)$$

mains. The supply line current (i_{sa}) is in phase with the phase voltage [Fig. 6(a)]. However, a small distortion is observed in the line current (<3%), which results in an overall input power factor equal to 0.972. The CSR ac current (i_{ia}) and dc-bus voltage (v_{dc}) are of the PWM type [Fig. 6(b) and (c)], due to the use of the SVM technique. Thus, the distortion introduced on the load and supply system is minimized. Both d and q actual current components are equal to the references, hence, unity DPF is achieved [Fig. 6(d)]. It should be noted that there is a fair amount of noise, both radiated and conducted, in a power converter environment. It may, therefore, be difficult to record clean signals. However, measuring voltages directly across capacitors minimizes noise pickup.

Finally, a step increase in $i_{sq,ref}$ at $t = 13$ ms (from 0 to 3 A), while $i_{sd,ref}$ is set at 4 A, illustrates key dynamic features. Fig. 8 shows the d and q line current references and actual values. It can be seen that the d component is not modified during the transient [Fig. 8(a)]. This confirms the decoupling and independent control of the active and reactive power. The settling time is found to be approximately 5 ms [Fig. 8(b)], which confirms the validity of the design guidelines of the line current component controllers. The results all indicate that the damping resistors on the input filter are no longer necessary. The required damping is supplied by the state variable feedback compensation. Similar tests were done for different operating points and they all showed similar transient responses, which confirms full linearization obtained through the input transformation.

VIII. CONCLUSIONS

Simple and direct on-line control of a current-source rectifier is designed to regulate the ac line currents directly in the stationary abc frame. This paper has demonstrated the superiority of the proposed control technique, which features the following: 1) control in a rotating dq frame; 2) a decoupling between d and q components; and 3) the use of a nonlinear transformation to linearize the model. Furthermore, the use of DSP hardware and software greatly simplifies the implementation of the proposed control technique. It also allows integration of control functions and PWM pattern generation. Results on a 2-kVA prototype indicate the following: 1) complete and accurate displacement power factor control; 2) fast, accurate, and independent control of the d and q line current components; and 3) low-input current harmonic distortion.

APPENDIX

INTERNAL DYNAMICS STABILITY ANALYSIS

The *internal dynamics* corresponds to the dc-link current differential equation given by

$$\frac{d}{dt} i_{dc} = \frac{3}{2} \frac{1}{L_{dc}} G_{ac} (m_d v_{cd} + m_q v_{cq}) - \frac{R_{dc}}{L_{dc}} i_{dc}. \quad (A1)$$

On the other hand, the modulating vector ($[m]_{dq}$) given by (18) can be written, using (19), as (A2), at the top of the page.

The *internal dynamics* (A1) is stable if the dc-link current (i_{dc}) is bounded for any arbitrary but bounded modulating vector ($[m]_{dq}$). However, there is an intrinsic property of nonlinear systems of considering the *internal dynamics* when the control inputs $[u]_{dq}$ are such that the outputs ($[i_s]_{dq}$) are maintained constant (i.e., $[i_s]_{dq} = [I_s]_{dq}$) [15]. Consequently, their time derivatives are also zero. Under these circumstances, the capacitor voltages are also constant (i.e., $[v_c]_{dq} = [V_c]_{dq}$). Thus, the modulating vector $[m]_{dq}$ can be written as

$$[m]_{dq} = \frac{1}{G_{ac}\omega_r^2 i_{dc}} \begin{bmatrix} I_{sd}(\omega^2 + \omega_r^2) + \frac{2\omega}{L_i} V_{cq} - \frac{\omega}{L_i} V_{sq} \\ V_{sq}(\omega^2 + \omega_r^2) - \frac{2\omega}{L_i} V_{cd} + \frac{\omega}{L_i} V_{sd} \end{bmatrix} \\ = \frac{1}{G_{ac} i_{ac}} \begin{bmatrix} I_d \\ I_q \end{bmatrix} \quad (A3)$$

where I_d and I_q are constants introduced to simplify the rest of the analysis. Replacing (A3) into (A1), we obtain

$$\frac{d}{dt} I_{dc} = \frac{1}{i_{dc}} \frac{3}{2L_{dc}} (V_{cd} I_d + V_{cq} I_q) - \frac{R_{dc}}{L_{dc}} i_{dc}. \quad (A4)$$

By defining $r = i_{dc}^2$, replacing it into (A4), and solving the resulting first-order differential equation, it is found that

$$r = \frac{3}{2R_{dc}} (V_{cd} I_d + V_{cq} I_q) (1 - e^{(-2R_{dc}/L_{dc})t}) + i_{dc}^2(0). \quad (A5)$$

Since $i_{dc} = \sqrt{r}$, the expression for the dc-link current becomes

$$i_{dc} = \sqrt{\frac{3}{2R_{dc}} (V_{cd} I_d + V_{cq} I_q) (1 - e^{(-2R_{dc}/L_{dc})t}) + i_{dc}^2(0)}. \quad (A6)$$

The expression for i_{dc} (A6) is bounded, since $\exp(-2R_{dc}/L_{dc}t)$ always converges. Therefore, the *internal dynamics* is said to be locally asymptotically stable [15]. Note that the load has been modeled by a resistor R_{dc} . The analysis to include active loads is beyond the scope of this paper.

REFERENCES

- [1] C. Namuduri and P. Sen, "Optimal pulse width modulation for current source inverters," *IEEE Trans. Ind. Applicat.*, vol. IA-22, pp. 1052–1072, Nov./Dec. 1986.
- [2] H. Karshenas, H. Kojori, and S. Dewan, "Generalized techniques of selective harmonic elimination and current control in current source inverters/converters," *IEEE Trans. Power Electron.*, vol. 10, pp. 566–573, Sept. 1995.
- [3] P. Enjeti, P.D. Ziogas, and J. Lindsay, "A current source PWM inverter with instantaneous current control capability," *IEEE Trans. Ind. Applicat.*, vol. 27, pp. 893–643, May/June 1991.
- [4] Y. Sato and T. Kataoka, "State feedback control of current type PWM ac-to-dc converters," *IEEE Trans. Ind. Applicat.*, vol. 29, pp. 1090–1097, Nov./Dec. 1993.

- [5] X. Wang and B. Ooi, "Real-time multi-DSP control of three-phase current-source unity power factor PWM rectifier," *IEEE Trans. Power Electron.*, vol. 8, pp. 295–300, July 1993.
- [6] S. Hiti, V. Vlatkovic, D. Borojevic, and F. Lee, "A new control algorithm for three-phase PWM buck rectifier with input displacement factor compensation," *IEEE Trans. Power Electron.*, vol. 9, pp. 173–180, Mar. 1994.
- [7] Y. Sato and T. Kataoka, "A current type PWM rectifier with active damping function," *IEEE Trans. Ind. Applicat.*, vol. 32, pp. 553–541, May/June 1996.
- [8] N. Zargari and G. Joós, "An on-line operated near unity power factor PWM rectifier with minimum control requirements," in *Conf. Rec. IEEE IECON'94*, 1994, pp. 593–598.
- [9] J. Holtz, "Pulsewidth modulation—A survey," *IEEE Trans. Ind. Electron.*, vol. 39, pp. 410–420, Oct. 1992.
- [10] V. Vlatkovic and D. Borojevic, "Digital-signal-processor-based control of three-phase space vector modulated converters," *IEEE Trans. Ind. Electron.*, vol. 41, pp. 326–332, June 1994.
- [11] J. Espinoza and G. Joós, "Current-source converter on-line pattern generator switching frequency minimization," *IEEE Trans. Ind. Electron.*, vol. 44, pp. 198–206, Apr. 1997.
- [12] M. Kazmierkowski and M. Dzieniakowski, "Review of current regulation methods for VS-PWM inverters," in *Conf. Rec. IEEE ISIE'93*, 1993, pp. 448–456.
- [13] D. Liebal, P. Vijayraghavan, and N. Sreenath, "Control of dc-dc buck-boost converter using exact linearization techniques," in *Conf. Rec. IEEE PESC'93*, June 1993, pp. 203–207.
- [14] P. Rioual and H. Poulliquen, "Non linear control of PWM rectifier by state feedback linearization and exact PWM control," in *Conf. Rec. IEEE PESC'94*, June 1994, pp. 1095–1102.
- [15] J. Slotine and W. Li, *Applied Nonlinear Control*. Englewood Cliffs, NJ: Prentice-Hall, 1991, ch. 6.
- [16] R. Dorf, *Modern Control Systems*, Reading, MA: Addison-Wesley, 1992, ch. 4.



interests include the modeling and control of static power converters and systems.

José R. Espinoza (S'93–M'98) was born in Concepción, Chile, in 1965. He received the Eng. degree (with first-class honors) in electronic engineering and the M.Sc. degree in electrical engineering from the University of Concepción, Concepción, Chile, in 1989 and 1992, respectively, and the Ph.D. degree in electrical engineering from Concordia University, Montreal, P.Q., Canada, in 1997.

He is currently an Assistant Professor in the Departamento de Ingeniería Eléctrica, Universidad de Concepción, Concepción, Chile. His research



Géza Joós (M'78–SM'89) received the M.Eng. and Ph.D. degrees from McGill University, Montreal, P.Q., Canada, in 1974 and 1987, respectively.

Since 1988, he has been with the Department of Electrical and Computer Engineering, Concordia University, Montreal, P.Q., Canada, where he is engaged in teaching and research in the areas of power converters and electrical drives. From 1975 to 1978, he was a Design Engineer with Brown Boveri Canada and, from 1978 to 1988, he was a Professor at the Ecole de Technologie Supérieure, Montreal, P.Q., Canada.